Trail Erosion Analysis Using Close-Range Structure-From-Motion Photogrammetry

Nicholas Hosek

Submitted in partial fulfillment of
the requirements for the degree of
Earth Sciences honours

Dalhousie University

March 2016

Distribution License

DalSpace requires agreement to this non-exclusive distribution license before your item can appear on DalSpace.

NON-EXCLUSIVE DISTRIBUTION LICENSE

You (the author(s) or copyright owner) grant to Dalhousie University the non-exclusive right to reproduce and distribute your submission worldwide in any medium.

You agree that Dalhousie University may, without changing the content, reformat the submission for the purpose of preservation.

You also agree that Dalhousie University may keep more than one copy of this submission for purposes of security, back-up and preservation.

You agree that the submission is your original work, and that you have the right to grant the rights contained in this license. You also agree that your submission does not, to the best of your knowledge, infringe upon anyone's copyright.

If the submission contains material for which you do not hold copyright, you agree that you have obtained the unrestricted permission of the copyright owner to grant Dalhousie University the rights required by this license, and that such third-party owned material is clearly identified and acknowledged within the text or content of the submission.

If the submission is based upon work that has been sponsored or supported by an agency or organization other than Dalhousie University, you assert that you have fulfilled any right of review or other obligations required by such contract or agreement.

Dalhousie University will clearly identify your name(s) as the author(s) or owner(s) of the submission, and will not make any alteration to the content of the files that you have submitted.

If you have questions regarding this license please contact the repository manager at dalspace@dal.ca.

Grant the distribution license by signing and dating below.

_____ _____

Name of signatory Date

Abstract

Measuring millimeter-scale changes in surface topography, in the field, is an important challenge for understanding numerous geomorphic processes, particularly for surfaces which evolve rapidly or for which quantitative prediction and/or measurement-directed land management decisions are necessary. Natural-tread recreational trails are an example of such a surface, as they evolve from factors that include trail design and construction, substrate, climate, and disturbance by users and natural processes on trail tread dynamics. Understanding trail dynamics is currently hindered by the measurement methods that are slow to collect, particularly in remote backcountry settings, are only 1 or 2 dimensional, and yield accuracies of only centimeters to decimeters. Our aim is to develop, test and apply structure-from-motion (SfM) photogrammetry as a new method of quantifying trail surface change in 3D. We sampled with photographs (254-400), pre-, during- and post- impact conditions, three sections (clay loam, grass and gravel surfaces) of a trail tread at York Redoubt Park, Nova Scotia in November, 2015, where a cyclocross race was taking place. Changes in sub-millimeter resolution DEMs of the clay loam surface, rendered in Agisoft Photoscan Professional, caused by 1186 passes by cyclists were analysed using DODs (Difference of DEMs), transect mean elevation change, flow path vectors, sinuosity and height distribution functions. The grass and gravel surfaces did not reconstruct fully (<20%) in Agisoft Photoscan Professional due to the small-scale repeating pattern of the grass and blurry images from water droplets on the camera lens, and were discarded from all subsequent analysis. Difference of DEMs and sign plots revealed that cyclists locally displace material outward from the trail axis as a cumulative effect of rutting. Transect mean elevation change and first standard deviation patterns can show that roughness increases as surface degradation increases from immediate impacts and becomes smoother as the surface relaxes. The total volume change (+446 mm^3 for pre to during, -790 mm^3 for during to post, and -310mm^3 for pre to post) was low given the study area (3.352m x 1.118m of trail), indicating material was moved within rather than lost from the trail. Flow paths (topographic gradients) showed rutting along the trail axis impeded water flow perpendicular to and off the trail, but may amplify along-trail flows and rilling. Mean sinuosity of the entire surface changed little (1.09 for pre-, 1.13 for during- and 1.14 for post-), similar to earlier 2D measurements in Nova Scotia. Limitations to our results include difficulty using fixed control points on the imaged surfaces, because the surface is so dynamic and user-safety precludes fixed rigid markers. Our results show that sub-millimeter resolution DEMs, rendered from modern structure-from-motion photogrammetry software can be used to characterize trail surfaces and provides a new approach to trail and land management.

Keywords: *structure-from-motion, erosion, trail, digital elevation model, geomorphology,*

Acknowledgements

This study was possible due to the efforts of many different people. Notably, my supervisor, Dr. Lawrence Plug who helped me with editing, acquiring references, data collection, Matlab scripting and providing me with office space to work. Also Thomas Duffett and Charlie Walls who helped with brainstorming, and managing computer resources and my colleague Sean Kelly who assisted in concept brainstorming. Special thanks goes to Shannon Murphy, Angela Grueneberg, Randy Hosek and Ingeborg Lang for continued support throughout the study.

Table of Contents

Table of Figures

List of Tables

1.0 Introduction

Tripling of the human population in the last century has had a profound impact on Earth's landscape. Agricultural intensification driven by urbanization[*Lambin et al.*, 2001] has altered land-cover and led to reduction in unaltered land, such that anthropogenic landscapes now span approximately 50% of continental surfaces. Backcountry areas have been deforested for agriculture, subdivided for housing and commercial businesses, or fragmented by access roads. For example, the Great Lakes area in North America has seen a 6087 km^2 decrease in forested land, an increase of 5722 km^2 in agricultural land and an increase of 632 km^2 of urban area between 1970 and 1990-2000 [*Létourneau*, 2010]. Remote land protection has been addressed through the creation of managed parks and other land management categories (e.g. Wilderness, National Forests) depending on region and national policies that variably balance goals of preservation, resource extraction and other human uses including recreation.

Recent study of the human relationship with nature has suggested that active recreation in natural spaces, facilitated by parks, is vital to human health and well-being [*Maller et al.*, 2010]. Now more than ever, land management will become imperative to preserving the remaining wild places while simultaneously integrating human uses that have been identified as important for mental and physical health. However, as recreational uses in natural areas increases, particularly on trails, effects of use can include physical erosion and impacts on vegetation. As trails are used, they degrade [*Marion*, 2006], which poses maintenance costs, reduces the utility of trails for providing experiences important for mental and physical health, and degradation of a natural environment (albeit at very local scales compared to other human activities). User-caused erosion may also trigger, or increase rates of, natural erosional processes such as rilling on

hillslopes. Future land management will require tools capable of accurately and efficiently recording trail degradation and changes, adequately assessing risk (both ecological and user related), planning appropriate preventative maintenance and engineering trail designs which are durable under high rates of use. The current tools do not address the before mentioned criteria. I propose to explore and develop a new approach to analysing recreational trail erosion through surface modelling.

This study attempts to analyse user-induced trail erosion by comparison of high-resolution digital elevation models of the trail micro-topography. The study area is York Redoubt Park, Nova Scotia during a cyclocross race event chosen because the event provided a known number of trail users, over a short (days) time period. The surfaces are digitally imaged hundreds of times at close range using a visible light, still camera capturing every perspective. The surface is imaged pre, during and post change. Structure-from-motion photogrammetry software is used to render DEMs of the trail surfaces from the image sequences. A broad suite of metrics drawn from geomorphology and other disciplines is applied to DEMs and DODs (Difference of DEMs), to attempt to quantify the spatiotemporal patterns of surface roughness, soil loss and displacement and water flow paths. The changes we observe in the DEMs show physical and temporal properties of trail erosion. Overall, we find the method to be a promising approach to advancing understanding of erosion, but also discuss its current limits.

This approach of characterising direct user impact on trail erosion will provide land managers and planners with access to intuitive 3D graphical representations of the trail and trail statistics for immediate and archiving purposes. They will have the ability to characterise their trails with minimal field work in a short period of time. This method requires only a camera to be

taken into the field, allowing analysis of any accessible trail. Development of this method may improve trail characterization and the interpretation of trail conditions.

Summary of Literature

2.1 Physical Erosion

Increases in trail traffic and new uses in recent decades (such as mountain-bikes and all-terrain vehicles) have motivated the study of trail erosion, to better understand the effects of different users, substrate types, slope gradients, climate and other factors. Numerous methods have been introduced in order to measure physical trail erosion. Research has followed either a point-sampling method or a census-based method [*Leung and Marion*, 1999]. Sampling-based approaches use a random or systematic interval scheme to determine where to sample data, and are best suited for collecting measurement data about specific trail characteristics on physically or remotely accessible trails. Census-based methods are more useful in quantifying visitor volumes, trail dimensions and assessing trail problems [*Leung and Marion*, 1999]. This method uses results from analog or web-based polls, or from direct interactions with users.

Indicators of trail soil erosion: maximum incision and cross-sectional area, were measured by using a systematic interval sampling method using a taut string strung perpendicular to trail tread in conjunction with a series of beads outlining the micro-topographic features of the trail to establish transect, recorded with photographs [*Marion*, 2006]. This device is very practical and easy to use in all locations, however the resolution of data is limited by to size and number of beads used to identify the trail surface. The cross-sectional area (mean soil

loss) suggests that ATV (246 in^2) and horse trails (150 in^2) are more severely degraded than hiking (19 in^2) and biking trails (6 in^2). Another approach, by problem assessment method provided census data on conditions, design and maintenance of the trail. This approach also revealed that ATV and horse trails experienced greater physical erosion than hiking and biking trails. Marion [2006] suggests that the type of use rather than the amount use is the greater determinant of trail degradation.

Water runoff volume and sediment yield increase with trail degradation [*Wilson and Seney*, 1994]. Wilson & Seney [1994] used an extensive method whereby 108 sample areas on existing trails in or near Gallatin National Forest, Montana, were treated with a modified Meeuwig drip-type rainfall simulator and runoff catchment device, and 50 passes by hikers, bikers, horses, motorcycles and off-road bicycles, before and after water treatment, in order to determine relative user impacts. No significant relationships were found between water runoff and: soil texture, antecedent soil moisture, soil resistance, trail roughness or slope. Ponding and infiltration is facilitated by increased surface roughness reducing runoff [*Wilson and Seney*, 1994]. Wilson & Seney [1994] suggested that perhaps trail roughness was not measured often enough to represent the micro-topography of the trail. The distribution of soil loss/deposition is strongly related to the local geomorphology, such as slope and drainage condition [*Tomczyk and Ewertowski*, 2012]. Other results showed that soil moisture contributed to reduction in soil resistance and ability to support a moving load which led to increased sediment yield on pre-wetted test sites. This was especially true for horse and hiker use, whereas motorcycle and bicycle use showed the least increase in sediment yield.

Trail width and maximum trail incision were measured along three slope gradient classes (<5%, 5-10% and >10% grade) using a point-sample system within 5 common ecological

regions in the southwest U.S. [*White et al.*, 2006]. Trail width was measured to the nearest inch perpendicular to trail tread between trail boundary points, marked with temporary stakes, defining the area where >90% of use had occurred. This region was estimated visually by interpreting cover type, composition and vegetation height. A trail-transecting nylon cord was strung between the trail boundary points and the maximum trail incision was measured at the maximum depth from the cord to the trail surface, to the nearest quarter inch. At each sample point a digital image was taken and the location recorded using a GPS receiver. It was found that trail width was significantly higher in the Arizona / New Mexico Mountains compared to the other test regions in this study. White et al., 2006, suggested that a variance in vegetation, soil, user-related variables or management may have been the cause of the increased trail width, but without proper controls and further study, the factors are difficult to quantify. There was no significant relationship between average trail width and slope of the trail. However, maximum trail incision increased significantly as slope increased for all sample areas. Slopes of 5-10% and >10% had larger maximum trail incision (ranging from 1.14-2.00 in. and 1.00-2.20 in. respectively) whereas the <5% slopes were not as deeply incised (ranging from 0.78-1.73in.).

Point sample trail analysis using a cross-beam and rod device at Nine-Mile river trail [*Jacques*, 2011] concluded that bikers and hikers interact very differently with the trail surface. Topographic transects across trail surfaces were measured with 2cm horizontal resolution and 1mm ±2.5 mm vertical resolution using a horizontal beam suspended across the trail with threaded rods at 2 cm intervals. The lengths of the rods are capable of matching the trail topography by rising or falling within their respective holes. A high resolution digital photograph of the beam and rods which captures the measurement which is analysed later. This device is useful for quickly acquiring coarse transect data, but is awkward to carry and can be difficult to

match set up location if temporal data is desired. Jacques [2011] found that bike use on trails results in rutting features whereas hiker use results in compaction and trail widening. Sinuosity of the trail surface (the ratio of length along trail topography and the Euclidean distance) was calculated before and after trials of hikers followed by bikers, and of bikers followed by hikers. They found that the roughening effect on the trail surface of when bikers travelled the surface before hikers, was greater than when hikers travelled first. However, the average sinuosity of walking (1.031) was only marginally less than the sinuosity of biking (1.034) and the average change from the baseline sinuosity to the post-trial sinuosity was actually a smoothening trend from 1.037 to 1.034. There was little sinuosity correlation between the baseline test and the trials and a strong correlation between the two trials. Jacques [2011] proposed that this may be because the natural roughness of the transects occur at different locations than those affected by users. This suggests that the user induced change does not directly amplify the deterioration of the trail, but rather increases the deterioration of new areas [*Jacques*, 2011].

Jacques [2011] also attempted low-angle LiDAR trail imaging of the rutted surface but results were inconclusive due to the device being positioned too close to the trail surface (within 2m). This method has potential for successful data acquisition if proper positioning can be accomplished, but for field measurements in remote areas, current LiDAR devices may not be the most convenient due to their weight (>80 kg) and power demands, and need for proper stabilization and positioning tens of meters from the surface. LiDAR derived micro-topographic DEMs (digital elevation models) tend to have uncertain accuracy due to abiotic and biotic terrain factors, and tend to be over-smoothed minimizing trail roughness and reducing topographic complexity [*Brubaker et al.*, 2013].

Tomczyk and Ewertowski [2012] used Topcon electronic total station derived (optical surveys) DEMs and DODs to analyse micro-topographic changes and measure soil loss of trail surfaces affected by hikers and bikers in 12 test fields. Survey density was approximately 80 pickets per m^{-2} and DEMs with 1x1 cm pixel resolution were created from the surveys using inverse distance weighting interpolation methods. Ten test sites experienced soil loss while only two test sites experienced deposition during a 2 years period. Trail surface average net volumetric change varied from -0.035 m^3m^{-2} to +0.005 m^3m^{-2} per year and the mean amount of soil loss/deposition can vary up to 400% for a population of trail visitors and is not linearly-related to the volume of use [*Tomczyk and Ewertowski*, 2012]. Tomczyk and Ewertowski [2012] also suggest that soil properties, morphology of trail tread and local geomorphology contributed most to trail changes. Soil loss is hypothesized to be the most widespread trail impact by all users [*Olive and Marion*, 2009].

2.2 Vegetation impacts

Examining how the user impacts vegetation, and at what point use begins to affect landscape, is often expressed as an asymptotic and curvilinear relationship. This means that initially, impact on the landscape increases dramatically with relatively low increases in use, reaching a single asymptote near the top of the curve, where after increases in use affect the impact on landscape much less than before the proposed inflection point. Recent studies [*Cole and Monz*, 2004; *Growcock*, 2005] suggest a more sigmoidal response where the relationship follows a path where two thresholds are met. It is suggested that an initial increase in use affects impact very little, upon crossing the primary threshold, impact increase dramatically with an increase in use and finally upon crossing the secondary threshold, an increase in use brings again very little change in landscape impact. However, more sensitive methods of measurement and

improved experimental designs would be required to confirm this. Under low to moderate use on flat, smooth, dry terrain, bikers and hikers have similar trampling effects on vegetation [*Pickering et al.*, 2011]. Only under high use conditions and on sloped paths do cyclists' impacts exceed those for hikers. Both types of users cause a reduction in vegetation height, cover and species diversity while increasing litter and soil compaction [*Pickering et al.*, 2011]. Studies suggest that more experimentation is required, especially analysing riding styles, and correlating topography, ecosystems and weather conditions. Our study will focus only on physical erosion of trails but, notably, the method in principle can also capture vegetation distribution and change.

2.3 Structure-from-Motion

Photogrammetry is a technique for calculating angles and distances on photographs for cartography [*Slama*, 1980] and has evolved extensively since the invention of the airplane, high resolution cameras, powerful computers and satellites. The idea of using cameras to estimate topography from aerial and ground based photographs was explored by Jordan, Laussedat, Arago and Stolze in the 1840's[*Maybank*, 1993]. Marr & Poggio [1976] successfully digitized the photogrammetry method through the development of an iterative cooperative algorithm which searches for and matches unique points between 2 images and constructs a smooth disparity between them [*Columbia University*, 1999]. Digitally reconstructing structure from motion using algorithms was developed by Ullman in 1979[*Columbia University*, 1999]. These concepts evolved into modern structure-from-motion software packages such as VisualSfM (http://ccwu.me/vsfm/), Acute3D (https://www.acute3d.com/), PhotoModeler (http://www.photomodeler.com/), 3DF Zephyr (http://www.3dflow.net/) and Agisoft Photoscan (http://www.agisoft.com/) which are capable of reconstructing closed objects and planar surfaces in 3D. A sparse point cloud model is constructed by aligning the suite of images: estimating the

camera orientation and position for each image loaded. Control over the maximum number of feature points considered on every image (key point limit) and the maximum number of matching points for every image (tie point limit) allows for management of memory resources and of the desired reconstruction quality. Depth information (depth maps) for each camera angle is calculated using the estimated camera orientations and positions, and assimilated into a single dense point cloud. A polygonal mesh can be generated from either the sparse or dense point cloud, the dense point cloud yielding the more detailed result. Finally, the mesh may be textured and colored if desired to help in matching ground control points or measuring surface distances, or exported to a complimentary software for further analysis. Agisoft Photoscan Professional offers an additional feature which allows for DEM generation from the dense point cloud without the need for external software.

2.4 Geoscience Applications of SfM

Recent successful experimentation with structure-from-motion photogrammetric workflows has suggested that SfM-based 3 dimensional processing will be a powerful addition to remote sensing and has numerous applications in geoscience [*Westoby et al.*, 2012]. A study of apparent surface temperatures and hydrothermal heat fluxes at the Mammoth Mountain fumarole area on Mammoth Mountain, CA, combined SfM modelling with thermal infrared data [*Lewis et al.*, 2015]. Overlapping, offset, high resolution images captured during the daytime were used to construct DEMs and orthorectified (cm-scale accuracy) images of the area using the structure-from-motion photogrammetry software Agisoft Photoscan Pro software. Pre-dawn time-series thermal infrared images (mm-scale accuracy) captured from a ground based camera were also captured. The thermal infrared images were matched with the DEMs by established ground markers and were overlain on the DEMs. The results were 3D maps of apparent surface

temperature of the area which will be used to better understand volcanic processes, monitor volcanic activity, explore the effects of geothermal exploration and development and assessing available resources. Close-range imagery of a 250 m transect of the reef surface at Heron Reef, Great Barrier Reef was captured to produce DTMs and mm-scale orthophoto mosaics using Agisoft Photoscan Pro [*Leon et al.*, 2014]. The surface roughness (root mean square height, tortuosity index and fractal dimension), an important indicator of net carbonate production and reef growth and may be used to estimate the effects of climate change on coral reefs, was modelled and analysed from the high resolution DEMs. Recently, helicopter-mounted digital SLR camera was used to capture images of a 32 km section of the Middle Fork John Day River in Oregon in order to investigate channel morphology from DEMs exported from Agisoft Photoscan Professional [*Dietrich*, 2015].

Based on these new applications of SfM to geoscience research, I believe that structure-from-motion photogrammetry is an effective, low-cost method to model the morphology of surfaces in 3D and will become increasingly important in geoscientific research, exploration and land management.

Methods

3.1 Study Areas

The study surfaces for this research were selected based on their susceptibility to alter in response to dynamic processes within a short temporal scale. The data were collected on trail surfaces along a cyclocross circuit at York Redoubt Park, N.S. in November 2015, capturing the

pre-, during- and post-race conditions. The pre-imaging was conducted approximately 2 hours prior to the beginning of the race. The during-imaging was conducted at the end of the first race day with a second race day taking place the following day. The post-imaging was conducted one week after the race weekend. The temperature was 15°C and overcast for the pre-imaging, raining for the during-imaging and clear for the after-imaging. Three distinct surfaces were chosen for imaging. The first surface (S-1) is a consolidated, clay loam containing a few small embedded pebbles and approximately 25% organic material. It is bordered on one side by a variety of grasses and low shrubbery, and on the other side by a vertical, straight cement building wall spanning the entire length of the section. The trail surface slopes approximately 5.75° down trail along 315° strike flattening towards the top end of the study area to approximately 2.80°. The surface simultaneously slopes perpendicular to strike, beginning at approximately 3.50° and flattening near the top of the study area to approximately 1.35°. The study section is 3.39m long by 1.44m wide rectangular region of an unmaintained but well established trail. Three ground control points were positioned tightly along the cement wall with spacings of 1.67m and 1.72m respectively and one GCP was positioned perpendicularly 1.44m across from the first control point. The second surface (S-2) is a section of a man-made, unconsolidated, gravel (~2cm diameter) path bordered on both sides by short grass. It slopes approximately 3.10° to the northeast. The region is defined by 4 GCP's placed at the 4 corners of 2.67m long by 2.66m wide rectangular area. The third surface (S-3) is a section of short grass field sloping approximately 7.25° to the northeast. The region is bound by 4 GCP's positioned at the 4 corners of a 2.94m long by 2.82m wide rectangular area. It was hypothesized that these surfaces would represent a diverse enough example of surface complexities with which to test the SfM software and proposed analysis.

Sixty-six cyclists completed a mean of 11 laps each in the first race, between the pre- and during- measurements. For the second event it was 46 cyclists and 10 laps each. The disturbance was therefore at least 726 and 460 passes by bicycles with approximately 33 mm wide tires. An unknown but small number of spectators walked on the trail surfaces during the race. After the

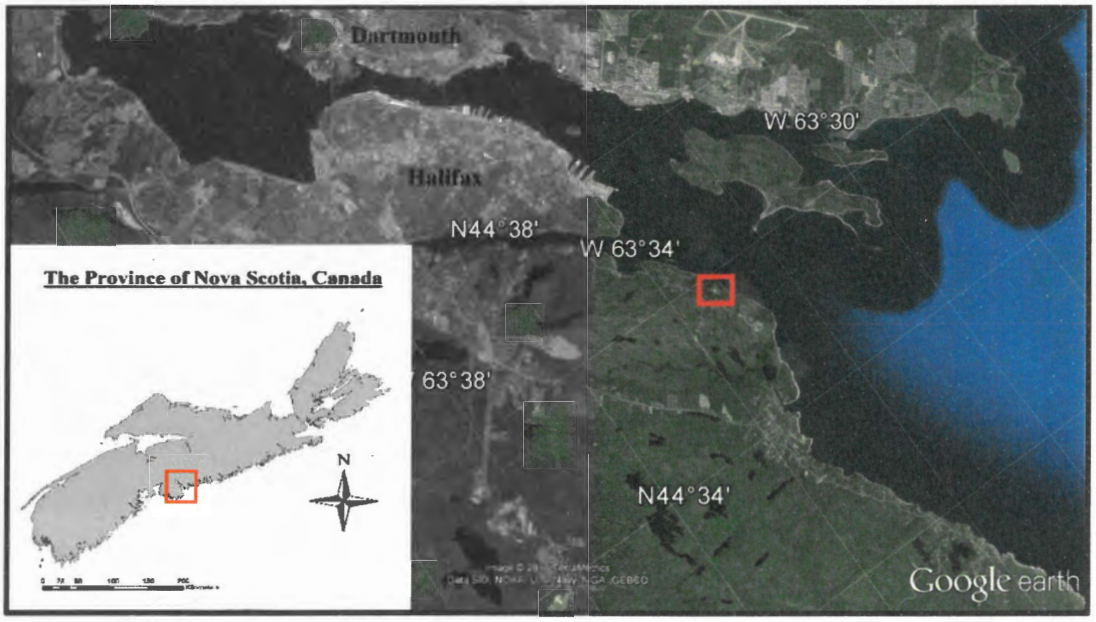

Figure 1. Location of study area. Red box in inset shows the location of the Halifax area within Nova Scotia. Red box in the aerial photograph shows location of York Redoubt Park.

second race, and before the post-images were acquired, a small population of daily joggers, walkers and dogs used the trail.

3.2 Hardware

Still images were captured using a Nikon D300 camera maintained at constant exposure settings for each scene. The hardware used to experiment with the various software workflows and perform analyses on the DEMs was a factory ASUS M32 platform with an Intel ® Core ™ i5-4460 CPU at 3.20GHz, 15.9GB of physical memory and 2048 MB of graphic memory. This

computer accomplished all necessary tasks although it is highly recommended to use a more suitable

Figure 2. Study sites at York Redoubt Park, Nova Scotia. Triangles show the location of the test surfaces.

architecture designed for 3D modelling and rendering, especially when using larger (>300 images) data sets, in order to reduce computing times, which reached 43 hours for a single image set.

3.3 Selection of SfM software

Experimentation began by using VisualSfM v0.5.26 (Wu, 2012). It is freeware, integrated software which combines structure-from motion and digital photogrammetry tools into one common Graphical User Interface. Feature detection was processed by SiftGPU (optional GPU-accelerated feature detection) and bundle adjustment calculated by PBA (a multicore bundle adjustment algorithm). The dense reconstruction module uses the embedded Yasutaka Furukawa CMVS/PMVS2 (Clustering views for Multi-view Stereo and Patch-based Multi-view Stereo

Software v2) tool to build the dense cloud. The point cloud was then exported to MeshLab v1.3.3 where the model surface was rendered into a 3D triangular mesh using a Poisson reconstruction. A third software would have been needed to build DEMs from the mesh. VisualSfM, offers extensive customizability enabling it to cater to many applications, but also required an advanced understanding of computer vision algorithms and photogrammetry parameters to operate. Instead, Agisoft Photoscan Professional Edition v1.2.2 build 2294 (64 bit) was chosen. It is a multi-view 3D reconstruction software containing Autodesk ® FBX ® code and native Agisoft photogrammetry algorithms which allows it to match points from image sequences, represents them as point clouds and builds DEMs (it is also capable of building meshes, textures, tiled models and orthomosaics). It was chosen due to its stability, simple GUI, ability to handle large data sets, integrated nature and excellent software troubleshooting team.

3.4 Data Acquisition

The resolution and accuracy of the DEMs are directly related to the selection of camera angles, the resolution of the images, the number of images and ground control point positioning. Photos had to be taken from as many perspectives as possible in order for the sequence to have complete spatial coverage. Each surface was imaged using two techniques to ensure that the raw image data contained equal amounts of complexity for all parts of the area. The first, was a grid pattern whereby images were captured facing an arbitrary frontside aspect, moving from left to right and breaking the area into 6 rows. At the top of the region, images were taken as the perspective changed to return imaging in the opposite direction to capture the arbitrary backside aspect of the surface (to maintain continuous overlap within the sequence) and breaking the area into another 6 rows. Upon arrival at the starting point, the second technique, a circular pattern of image collection, was used. Three successively shrinking circular paths starting from the exterior

perimeter of the area and working inward, were followed. We believe that the combination of the two techniques provided sufficient coverage and data about the surface. Images were shot at approximately 60 degrees from normal to the surface. Furthermore, a minimum 60% side overlap and 80% forward overlap was used to ensure that no area was left out. The images were captured at the finest setting on the camera to maximize resolution. Each surface was imaged no less than 250 times. Ground control points were established to serve as linear geomorphic markers of the bounds and quadrant off the surface to be imaged. The GCPs were 2cm by 2cm pieces of fluorescent orange flagging tape fixed to the ground using a washer and a stake. A minimum of 4 GCPs were used at each surface to have ample points for matching before, during and after models, and for scaling.

Our procedures for acquiring images rendered SfM results that were sufficient to quantify surface change, at least for surface S-1. Nonetheless, procedures could be modified for better results.

3.5 SfM Processing

Figure 3, lists the steps used in Agisoft Photoscan Professional to build DEMs from the suites of raw digital images. Italics denote user defined selections from drop down menus or a manual input.

3.6 DEM Normalization

Models were oriented according to a local coordinate system manually in Agisoft Photoscan Professional prior to building and exporting the DEMs. Matlab v8.6.0.267246 (64-bit) was chosen to analyse the DEMs. The DEMs required some alignment correction because their relative orientations set by hand in Agisoft were not perfectly congruent. The coordinates of the

ends of the cement wall used to align models, by rotating each a small angle (determined by *arctan(Δx,Δy)*) so the wall was aligned with the long axis of the model. The "during" scene was

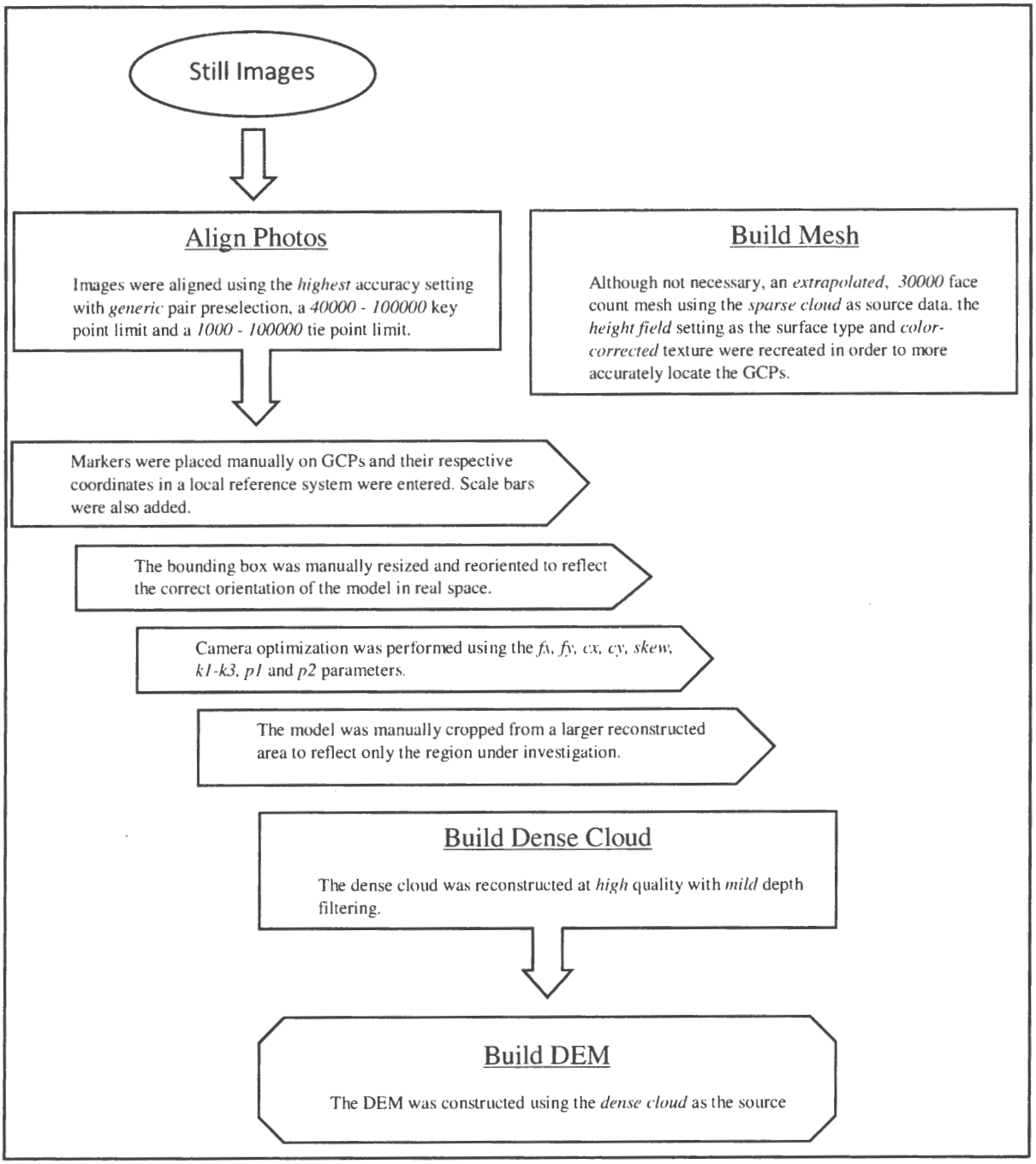

Figure 3. Steps used in Agisoft Photoscan Professional to build DEMs from still images.

very close to vertical and therefore did not require an angular correction. Each scene was rotated using a nearest neighbour interpolation. The regions were redrawn and the post-rotation coordinates were captured. Using these coordinates the images were cropped to a consistent dimension of 3352 x 1118 mm, chosen because it included only well-resolved SfM results. For vertical controls, three, 2 pixel x 20 pixel strips, parallel to the vertical concrete wall and approximately 3cm from the edge on the gentle outgrade, were manually selected, matching the x,y positions of each on all three scenes. These regions were selected because no observable deposition or erosion occurred during the study period, they are within an area that cannot be reached by bicycle tires, and because they are flat. Elevation of the "during" and "post" surfaces were adjusted so the mean elevation calculated from the datum strips of each surface matched the mean elevation of the datum strips in the "pre" surface. The lowest elevation in the pre-surfaces was as the 0 datum.

3.7 DEM Analysis

Normalized DEMs were examined using various topographic metrics. Algorithms written in Matlab were used to simplify the process. Results of these analyses will be discussed in Section 4.0. To simplify visualization, we calculated and plotted sign plots (*Figure* 9) which show where elevation change was positive, negative and where little to no change was observed. We also differenced the DEMs from each interval without value reclassification producing continuous scale DODs (*Figure 10*). This was accomplished by differencing the surfaces in each interval; subtracting corresponding pixel values of the earlier image from the later image. We classified changes of $<\pm 2.5$ mm as no change (zero value). Differenced values $>\pm 2.5$ mm were deemed significant and were classified according to sign. This represents bulk change. Transect mean elevation changes for each of the time intervals (pre-S-1 to during-S-1, during-S-1 to post-

S-1 and pre-S-1 to post-S-1) were plotted (*Figure 11*) using the mean and first standard deviation for each pixel column (down-axis of the trail) in the elevation change surface (DOD). Total volume changes of the trail surface were also calculated by summing all columns in the DOD array and then summing the resulting row (numerical integration). Flow path analysis methods by Costa-Cabral [1994] and Paik [2008] were reviewed, however our method needed modification due to the small area. The DEMs were rescaled from the native 1x1 mm resolution by a factor of 0.02, using a bilinear (2D) interpolation, into 50x50 mm regions because water drops are sensitive to cm-scale rather than mm-scale relief. The "gradient" function returned 2D arrays containing the x,y lengths for every vector representing a water flow path, which by using a "quiverplot" function were plotted (*Figure 12*). Sinuosity algorithms developed and tested by Jacques [2011] on tens of transects, provided the framework of our sinuosity analysis of 3352 transects, perpendicular to trail axis for each surface. The sinuosity of each row in the DEM array was calculated by dividing the sum of the Pythagorean distances between all pixels in a row by the straight line distances of the transects was plotted on one graph. The mean of the sinuosities for each of the surfaces were also calculated. Height distribution functions for pre-S-1, during-S-1 and post-S-1 were plotted on one graph using the "hdf2D" function, requiring surface heights and the number of bins to generate histograms which were then summed and normalized. The RMS (root-mean-square) of the height was calculated, calling on the "std2" function, which calculates the standard deviation of elements in the 2D array (i.e. the DEMs).

Results and Discussion

4.1 Qualitative observations of trail changes

Most trail analysis up until this study has relied heavily upon visual observations and simple devices. Features are interpreted by people and changes in surface morphology are attributed to various impacts.

The pre-S-1 trail surface (*Figure 4*) was relatively smooth and consolidated. The soil was wet to the touch and no rutting was present. The trail appeared stable, no soil was displaced as contact while walking was made, and no large obstructions such as boulders or roots were visible. Vegetation grew tall on the right edge of the trail and low grasses were found on either side of the main trail tread. The during-S-1 trail surface (*Figure 5*) changed significantly from the pre-S-1 surface. The trail became deeply rutted, especially to the right of the trail axis. The vegetation became trampled, in some cases removed entirely, and the trail tread widened. To the left of the trail axis noticeable splashing and accumulation of soil occurred. The substrate became saturated with rain and most of the trail became a slurry. Rain accumulation travelled downslope via the ruts caused by the bicycle tires but did not seem to contribute much to further incising the ruts as the water was running very slowly along the shallow slope. Some small pools of water accumulated downslope (further downslope than the extent of our study area, towards the top of our plots). The post-S-1 surface (*Figure 6*) was relatively dry and some relic rutting was identified to the right of the trail axis. However, it seemed that most of the roughness observed in the during-S-1 surface had smoothed. Furthermore, areas which accumulated soil in the during-S-1 had settled, such as the region to the left of the trail axis. Areas which were

Figure 4. Oblique view of pre-S-1.

Figure 5. Reverse-oblique view of during-S-1.

Figure 6. Oblique view of post-S-1.

excavated by ruts earlier appeared to have partially refilled with soil. In effect, the surface was relaxing in response to natural processes, namely gravity. There was also some new features which were not present in the during-S-1 image. The park is open daily and use following the cyclocross race appears to have been limited to dogs and their owners as no fresh ruts caused by bicycles were seen. The relaxation of the trail does not necessarily reflect only natural processes but also human impact. We believe that the influence of the walkers and dogs on the trail during the time between the during-S-1 and post-S-1 did not significantly hinder nor accelerate the surface relaxation process. Walkers and dogs probably had much less impact on the trail than cyclists, especially as their number was considerably less than the cyclists in the cyclocross race.

4.2 Surface reconstructions

The pre and during models were reconstructed for S-2 and S-3, and the pre, during and post models were reconstructed for S-1. The S-2-pre model was reconstructed with a high degree of accuracy however the S-2-during model was over-smoothed and large regions were extrapolated. The lack of feature detection and poor alignment was a result of distorted images from rain-spray on the camera lens. The S-3-pre and during models were reconstructed but due to the repeating nature of the grassy surface, Agisoft Photoscan failed to build complete models; only ~20% of the surface was reconstructed. It appears that a surface characterized by a repeating pattern with low color differentiation such as grass does not render completely. It was not possible to accurately build DEMs of the S-2 and S-3 models due to the poor nature of the reconstructions and therefore were omitted from further analysis. Only the S-1 reconstructions

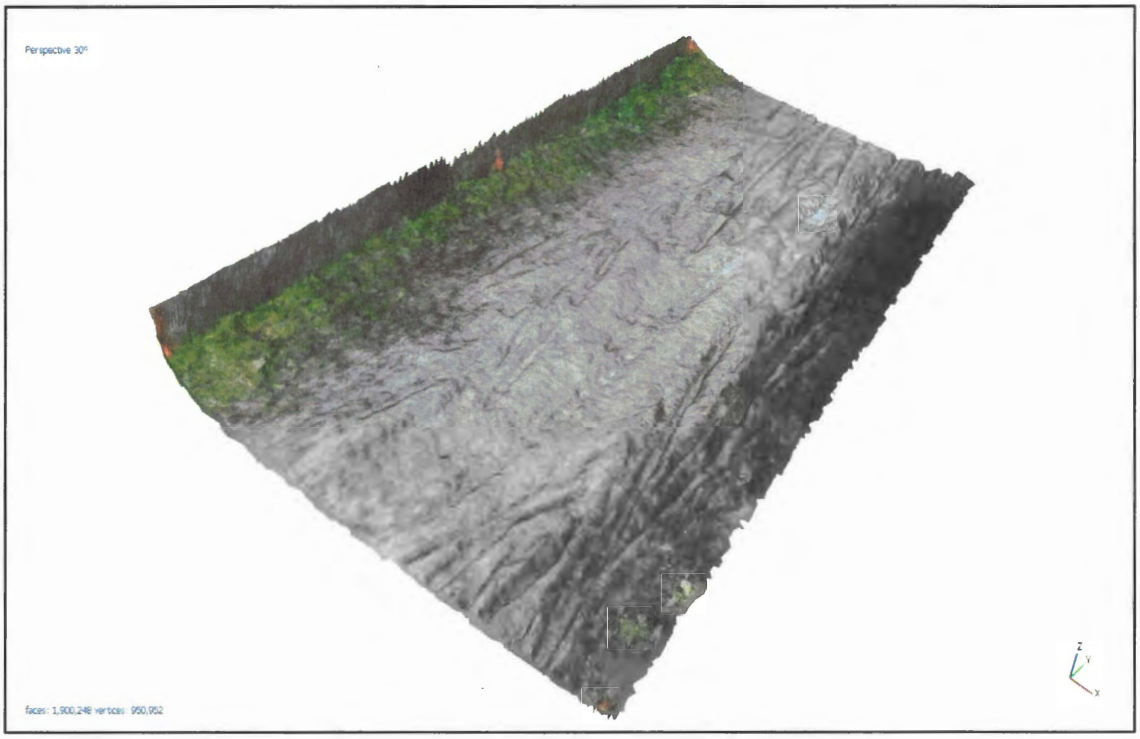

Figure 7. Oblique view of surface S-1 reconstruction of "during" model, rendered in Agisoft Photoscan Professional.

Table 1. Surface S-1 reconstruction parameters and results

Surface S-1			
Scene	Before	During	After
Cameras (number of images)	400	347	254
Point cloud	71977	34920	354083
Aligned cameras	380	184	254
Coordinate System	Local coordinates	Local coordinates	Local coordinates
Alignment parameters	*Highest* accuracy, *generic* pair preselection, *40000* key point limit and *1000* tie point limit	*Highest* accuracy, *generic* pair preselection, *40000* key point limit and *1000* tie point limit	*Highest* accuracy, *disabled* pair preselection, *100000* key point limit and *100000* tie point limit
Matching time[1]	1 hour, 4 minutes	41 minutes, 29 seconds	14 hours, 24 minutes
Alignment time[1]	1 minute, 39 seconds	39 seconds	3 minutes, 3 seconds
Optimization parameters	fx, fy, cx, cy, skew, k1-k3, p1 and p2	fx, fy, cx, cy, skew, k1-k3, p1 and p2	fx, fy, cx, cy, k1-k3, p1 and p2
Optimization time[1]	2 seconds	1 second	6 seconds
Depth maps	323	161	-*
Reconstruction parameters	*High* Quality and *mild* filtering	*High* Quality and *mild* filtering	*High* Quality and *mild* filtering
Processing time[1]	9 hours, 11 minutes	2 hours, 21 minutes	-*
Dense point cloud	12,551,664 points	9,636,433 points	14,892,904 points
Reconstruction parameters	*High* quality and *mild* depth filtering	*High* quality and *mild* depth filtering	*High* quality and *mild* depth filtering
Processing time[1]	1 day, 9 hours	2 hours, 28 minutes	11 hours, 15 minutes
DEM	3444 x 4885 pixels	3088 x 5896 pixels	3116 x 5004 pixels
Source data	Dense cloud	Dense cloud	Dense cloud
Interpolation	Enabled	Enabled	Enabled
Resolution	0.799 mm/pix	0.799 mm/pix	0.803 mm/pix
Resampled for analysis	1.00 mm/pix	1.00 mm/pix	1.00 mm/pix
Total processing time[1]	~43 hours, 16 minutes	~ 5 hours, 30 minutes	~*

**Depth maps were constructed however as a result of experimentation with mesh and texture generation, the technical data was overwritten before being recorded.*

[1]*The processing times reflect performance of hardware listed in Section 3.2.*

were chosen for DEM generation and statistical analysis (*Figure 7*). The reconstruction parameters and results of S-1 are listed in *Table 1*. Our experience is that SfM software can reconstruct trail surfaces which have repeating features that are less complex than grass blades but perhaps more complex than gravel. Further experimentation is required in order to better

understand the relationship between pattern complexity and the structure-from-motion reconstruction ability.

4.3 Digital Elevation Models

DEMs of the pre-, during- and post- S-1 surface were plotted (*Figure 8*). High resolution micro-topographic DEMs of a trail surface have never been previously collected, based on our reviews of existing literature. We chose to measure several metrics which we hypothesize may usefully characterize the surfaces. The reference DEMs (*Figure* 8) were cropped to an area with new dimensions of 3352 x 1118 mm (mention of DEMs in future analysis will refer to the cropped DEMs unless otherwise stated) in order to remove areas beyond the trail surface

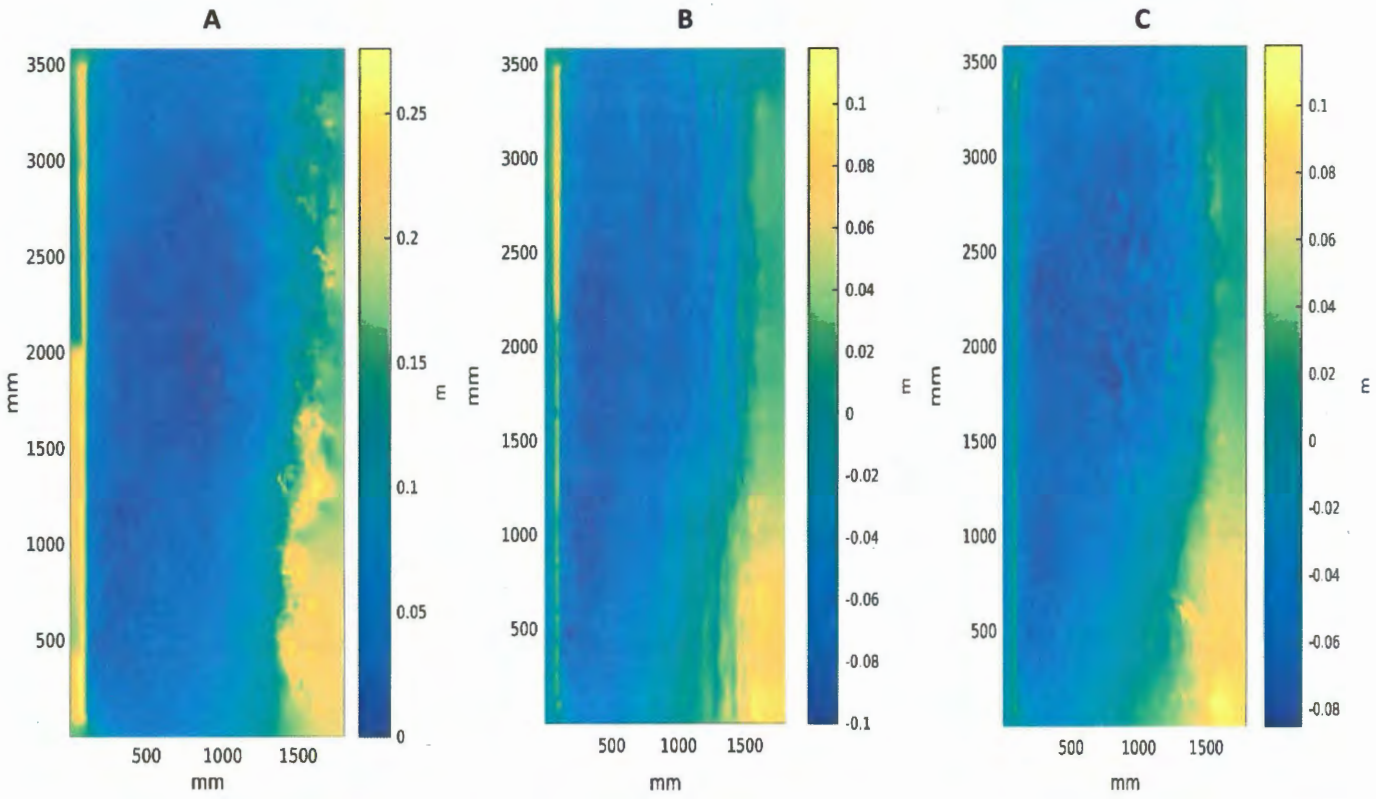

Figure 8. Reference DEMs using a blue-yellow color palette. A: pre-S-1, B: during-S-1, C: post-S-1. The wall is visible on the left. Blurred areas on the right and at the ends are the result of edge effects and incomplete vegetation reconstruction from SfM software, and are cropped from subsequent analysis.

including bordering vegetation and organic detritus on the right, and the vertical cement wall to the left. In so doing, some of the tread may also have been cropped out, especially for the post-surface. This was necessary because overhanging vegetation rendered unusable the SfM point clouds in these cropped regions. The 1 pix/mm resolution of the DEMs records spatial details which cannot be observed qualitatively. This data format can be used in immediate statistical analysis and is convenient for archiving.

4.4 Micro-elevation change and DODs

Changes in elevation along a trail are perhaps the most noticeable transformations of the surface as it degrades. These features can often be interpreted with the naked eye, however precise quantification is impossible without the help of measuring devices. In this case, sign plots (+/0/-) of micro-elevation change (*Figure 9)* and difference of DEMs (*Figure 10)* were drawn of pre-S-1 to during-S-1, during-S-1 to post-S-1 and pre-S-1 to post-S-1 to isolate areas of change. In the sign plots, blue pixels show surface elevation increase, red pixels show surface elevation decrease and white pixels show surface elevation with little/no change; defined as <2.5mm vertical change. In the DODs, the blue areas represent elevation drop and yellow indicates areas of elevation increase. Elevation increase probably indicates material accumulation and elevation decrease indicates material loss, although compaction and inflation, without movement, might also be a cause.

Elevation changes from pre-S-1 to during-S-1 (*Figure 9; B*) developed where expected. A decrease in elevation occurred in a band approximately 600mm wide along the axis of the trail. This was not recognized in the qualitative observations taken in the field, most likely due to the excessive muddiness of the surface. This area is interpreted as the result of overlapping

continuous, linear ruts (compacted or removed soil) running parallel to the trail axis. We suggest that the pattern of elevation decrease is consistent with that left by bicycle tires. The central nature of this pattern is caused by racers travelling along the most direct and safe route along the trail and in response to bicycle dimensions. A rider would not have been able to diverge far from the central area of traffic since the handlebars would have contacted with the vertical concrete wall on the left or the vegetation on the right. The distance from the central band of high traffic to the outer edges of the usable trail are a function of handlebar width. Adjacent to the areas of

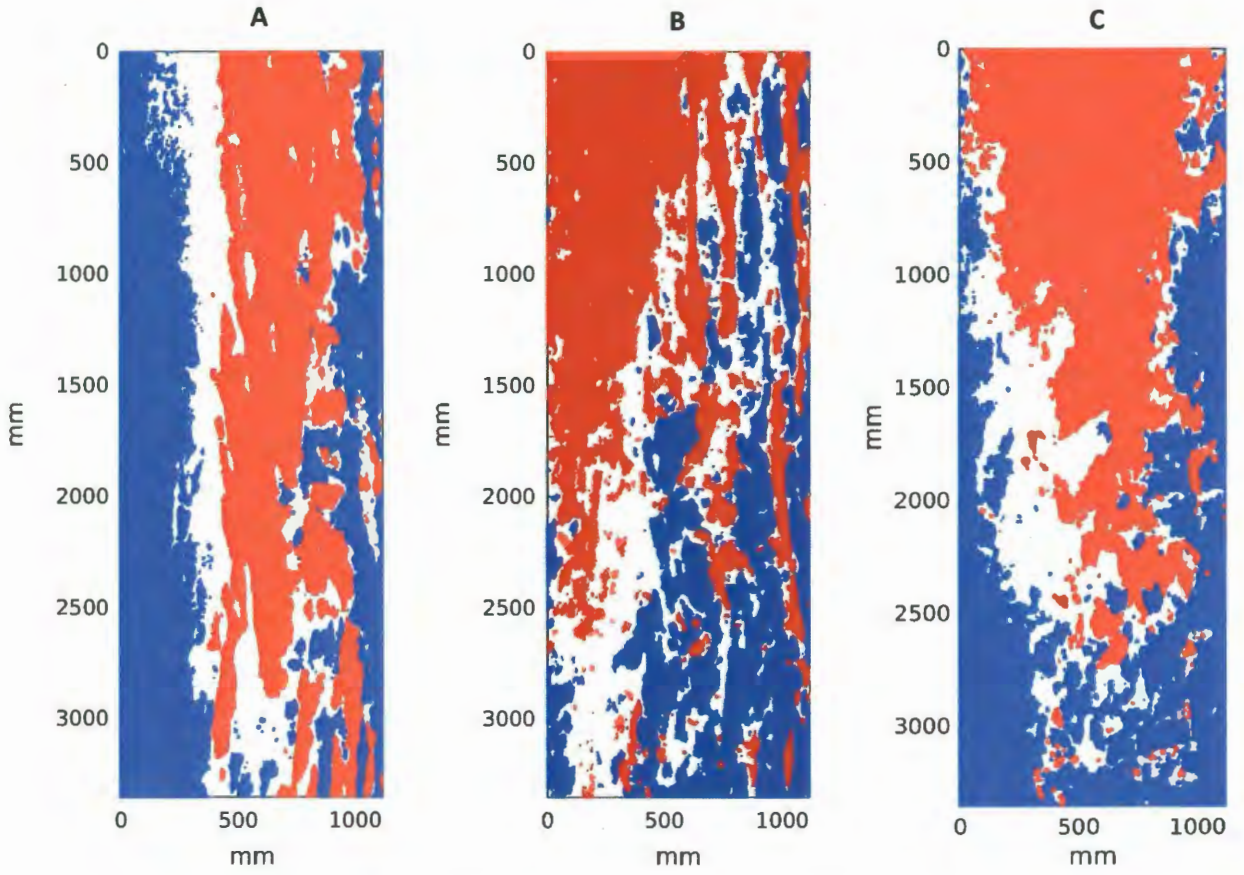

Figure 9. Sign plots showing changes in micro-elevation; positive elevation change (blue pixels), negative elevation change (red pixels) and little/no change in elevation; defined as <±2.5 mm vertical change (white pixels). A: pre-S-1 to during-S-1, B: during-S-1 to post-S-1 and C: pre-S-1 to post-S-1.

elevation decrease are areas of little change. To the left there is a band of approximately 150mm of little/no change and to the right there is no such band. We believe that due to the downward slope of the trail to the right, the wet and loosened material displaced by the bicycle tires tended

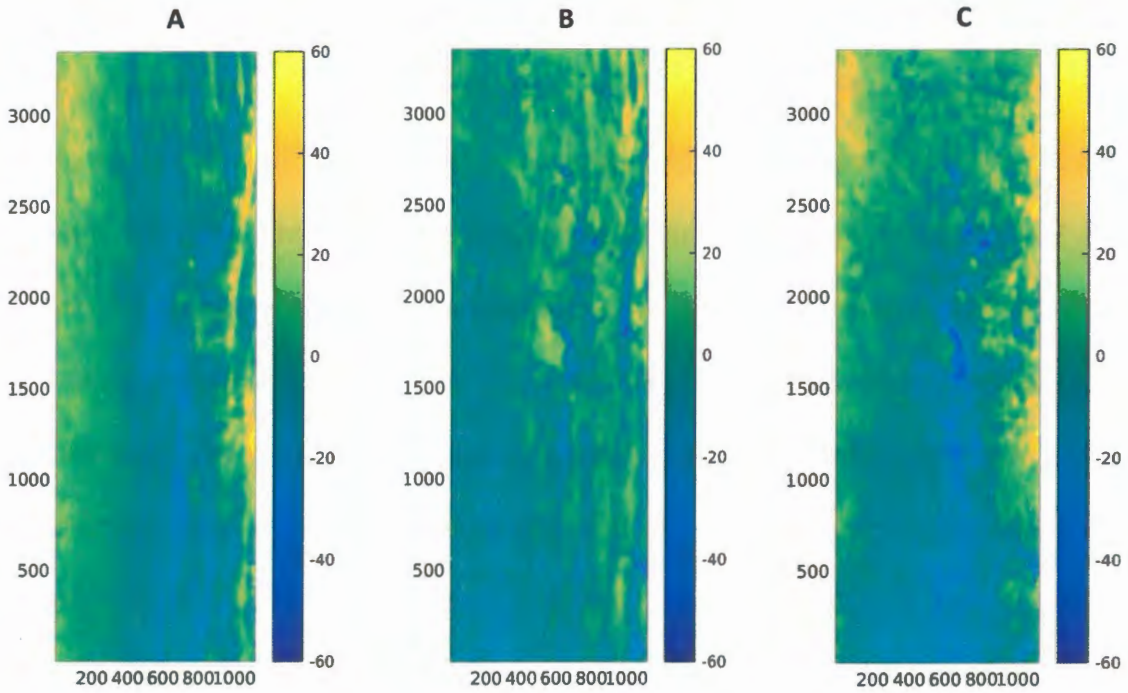

Figure 10. DODs using a blue-yellow color palette; blue pixels are areas of elevation decrease and yellow pixels are areas of elevation increase. A: pre-S-1 to during-S-1, B: during-S-1 to post-S-1 and C: pre-S-1 to post-S-1.

to fall and run to the right of the trail. Therefore the gradient between material loss and material accumulation is steeper on the right side than on the left. Also, this suggests that the gradient between material loss and material accumulation may be an indicator of slope. Areas of material accumulation occurred on both edges of the trail. This is consistent with the hypothesis that as bicycles travel along the trail, material is displaced from the central region outwards by the tires as they contact the surface forming ruts. The cumulative effect of many passes by bicycles is a general outward movement of material away from and perpendicular to the trail axis.

Elevation changes from the during-S-1 to post-S-1 reveal how trail impacts may begin to revert to a state of equilibrium over time. Some relic rutting is still present along the right margin of the trail however the relative distribution of other features has changed. The upper left corner of the trail area is now dominated by a decrease in elevation and separated by a mixed band of elevation increase, little/no change and elevation decrease, from the bottom right corner now dominated by increased elevation. This can be interpreted as a natural creep of material from the upper left corner of the area to the bottom right corner as the substrate settles and the surface relaxes. We believe that this natural shift of material is directly related to the slope of the trail. The mild gradient from elevation decrease to elevation increase suggest a gentle downward slope towards the bottom right of the surface. This slope is a relic feature consistent with the preliminary trail descriptions. Interesting features to note are the patterns of elevation increase and decrease along the right margin of the trail. These linear strips of elevation changes resembling ruts are actually the process of rutting in reverse. Areas which indicate elevation gain, were once ruts and areas reporting a decrease in elevation were the crests between the ruts. In effect, this is smoothening caused by natural surface relaxation.

The lack of distinguishable impact morphology defined by trail elevation changes after one week (*Figure 9; C*) suggests that the immediate impacts caused by bicycles (*Figure 9; A and Figure 10; A*) dissipate quickly when little to no trail traffic is present. Elevation decreased in the top and central area whereas elevation increased in the bottom and along the edges of the trail forming a V-shape. The slope of the trail and the distribution of elevation increase and decrease, suggests that the trail has experienced incision. However, it was not expected for material to accumulate up-slope. One possible explanation for this is that the material upslope (the bottom of the area) was more resistant to loosening on the race weekend due to improved drainage

conditions, leading to the areas downslope (top of the area) to be more saturated and more susceptible to erosion. However, on such a small-scale, this along-trail elevation undulation may not be significant enough to be correlated to slope and rather to a natural feature of common riding style (such as sudden breaking, swerving and acceleration) in this section of trail.

4.5 Transect mean elevation change

The mean and first standard deviation of mean elevation change, as measured perpendicular to the trail axis were drawn for the three time intervals (*Figure 11*). The relative size of the first standard deviation indicates the variability in mean elevation change between time intervals. The pre-S-1 to during-S-1 plot (*Figure 11; A*) reveals that the central area of the trail experienced elevation decrease while the trail edges experienced an elevation increase. This agrees with observations made in Section 4.4. The area of greatest incision is approximately at 700mm from the left extremity of the study area and is very close to being in the center of the trail, which appears to be the most direct and highest traffic race path. This concentration of traffic near the center of the trail is a function of bicycle dimensions and the protrusion of the handlebars as mentioned in Section 4.4. The standard deviation is close to the mean on the left of the path of maximum incision whereas on the right, the standard deviation is generally larger and more varied than the mean. The variability of surface change is greater on the right than it is on the left based on the relative sizes of the standard deviations (ranging from 2-8 mm on the left and from 6-18 mm on the right). We believe that this is because riders may have occasionally diverged to the right, travelling into the vegetation, but never so to the left to avoid collision with the vertical concrete wall. By this hypothesis, the left side of the trail is accumulating material relatively more evenly and consistently from splashing along the length of the trail, whereas the

right side of the trail is receiving splashing but is also being rode on; leading to a relatively more varied morphology.

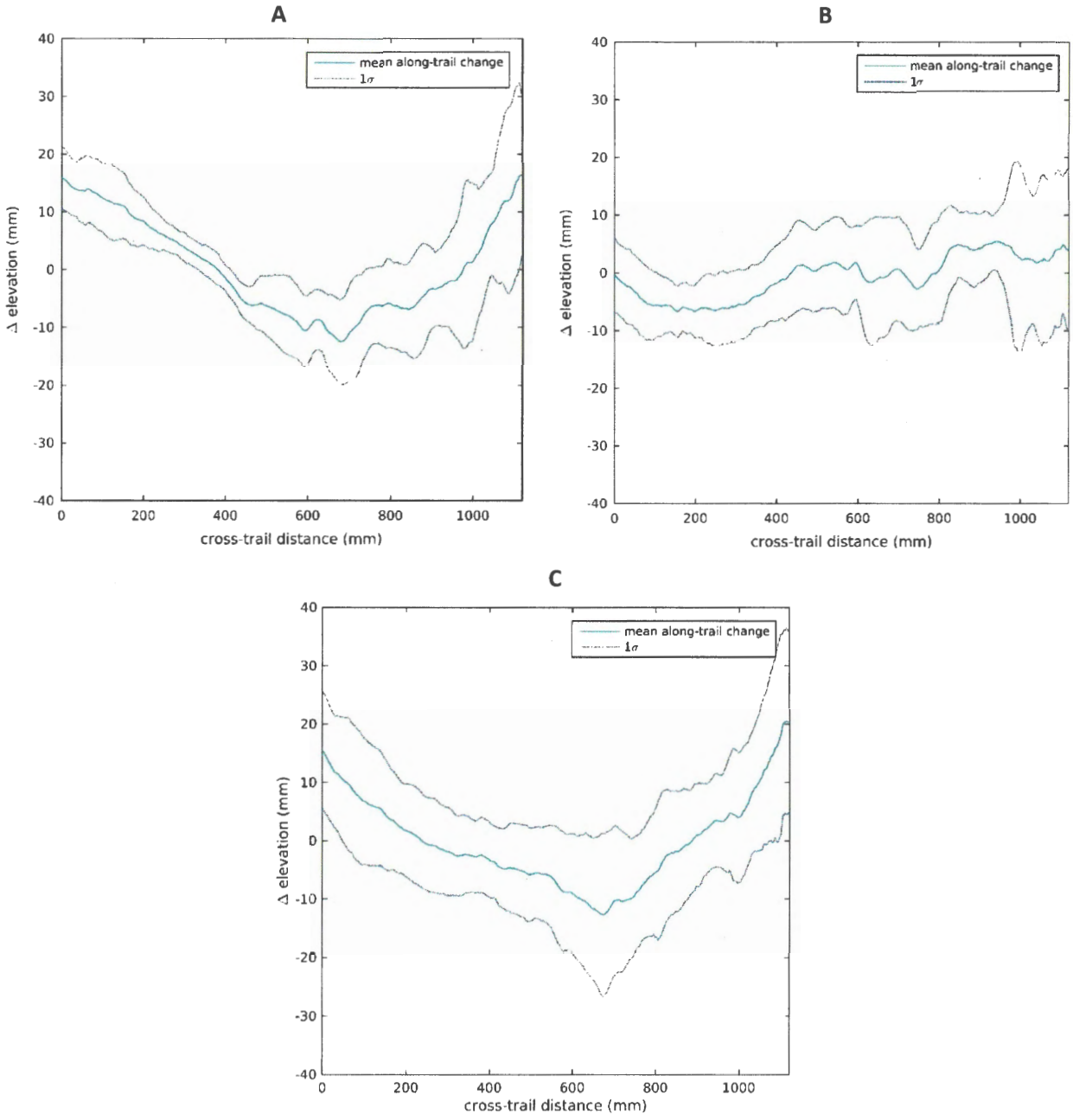

Figure 11. Transect mean elevation change. A: pre-S-1to during-S-1, B: during-S-1 to post-S-1, C: pre-S-1 to post-S-1.

The mean elevation change of the during-S-1 to post-S-1 interval (*Figure 11; B*) is less deviant (approximately -6-7mm) from zero elevation change than the pre-S-1 to during-S-1 interval (approximately -11-16 mm). The standard deviation ranges from approximately 8-15 mm and is more consistent than the pre-S-1 to during-S-1 interval. The gentler mean elevation change trend across the axis of the trail suggests a relaxation of the surface. A larger standard deviation on the right than to the left of the trail center is perhaps a feature of relic variability in elevation change described in the pre-S-1 to during-S-1 interval. Areas which had high standard deviations (for example on the right in the pre-S-1 to during-S-1 interval) now have relatively lower standard deviations. Areas which had low standard deviations (for example on the left in the pre-S-1 to during-S-1 interval) now have relatively higher standard deviations. Also, areas which showed positive mean elevation change in the pre-S-1 to during-S-1 interval show a negative mean elevation change in the during-S-1 to post-S-1 plots. Similarly, areas which showed negative mean elevation change in the pre-S-1 to during-S-1 plot show positive mean elevation change in the during-S-1 to post-S-1 plot. We believe that these transformations reflect the natural equilibration process of the surface (smoothening with time) in response to gravity, when impacts reduce or stop.

The mean elevation change of the pre-S-1 to post-S-1 (*Figure 11; C*) interval highlights the trail changes which occurred during the cyclocross race and did not smooth out completely after one week. There were significant changes especially to the axis and the edges of the trail. The greatest positive changes (material accumulation) occurred at the edges of the trail whereas the largest negative changes (material loss) occurred in the center of the trail. This is congruent with the sign plot (*Figure 9; C*) where soil was displaced outward. The standard deviation peaks at approximately 16 mm from the mean at the trail axis; the region of proposed maximum

incision, and the remainder of the transect has a more consistent standard deviation ranging from approximately 6-12 mm. The relative size and uniformity of the first standard deviation (variability of elevation change) shows that overall, the surface has undergone significant changes everywhere across the trail, despite the lack of visually identifiable relic impact features from the cyclists on the post-S-1 surface (*Figure 6 and Figure 8C*).

The total volume change was calculated for each interval using the transect data. A +446 mm^3 change in material volume was observed in the pre-S-1 to during-S-1 interval and the during-S-1 to post-S-1 interval yielded a -790 mm^3 change in material volume. The overall net change in material volume (pre-S-1 to post-S-1) was -310 mm^3. These changes in volume are not significant given the approximate 3.352 m x 1.118 m study area. Rather than a substantial net displacement into or out of the system we believe that the impacts of bike riding during the study period only contributed to local repositioning of material on the trail.

4.6 Flow path vectors

Trail surface disturbances by users causes topography that influences the paths of subsequent water flows. Since the trail surfaces have many outlets along all four edges of the surface and numerous closed basins, a traditional drainage basin flow path modelling tool such as ArcGIS Rivertools would not suffice. Instead, we decided to model gravitational gradients that drive surface water flow. Local gradient vectors for 50x50 mm regions were calculated instead of using the native 1mm resolution because water drops are sensitive to cm-scale, not mm-scale relief and vector arrows would not be visible for a 3352 x 1118 array. Although the results are not true flow paths, the orientation and length of the vectors show the direction and relative erosive energy that water has as it flows across the surface. The pre-S-1 flow path gradients (*Figure 12; A*) represent what one might expect by simply looking at the surface with

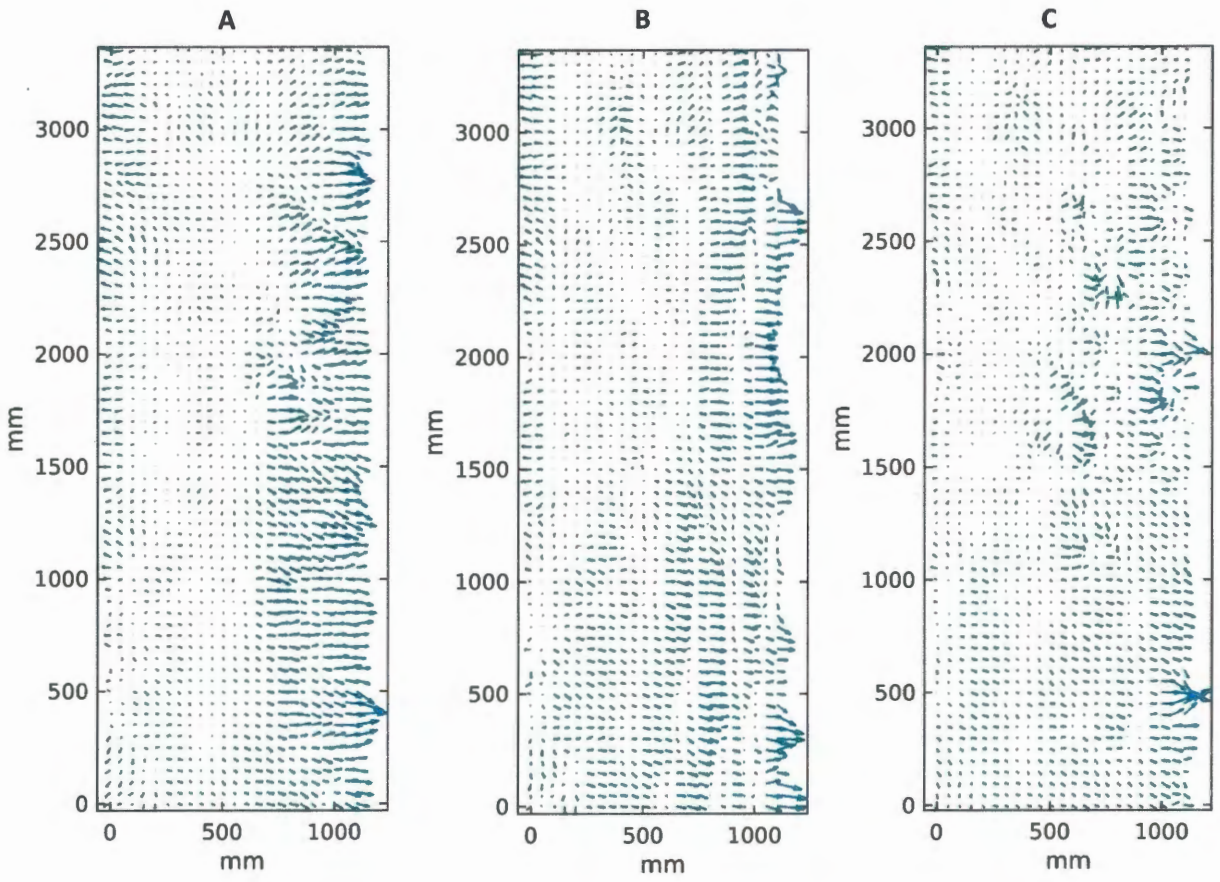

Figure 12. Flow path vectors models; A: pre-S-1, B: during-S-1, C: post-S-1.

the naked eye. The connected regions of aligned, large magnitude vectors on the right of the trail indicate that the erosive potential is greatest in this region. Furthermore, when compared to the during-S-1 and post-S-1 surfaces, pre-S-1 has the greatest erosive potential, owing to greater gradients and focused, well-connected gradient vectors. We believe that since this surface is smooth, and free of obstructions such as ruts, water will respond more easily to gravitational gradients (slope) and thus the potential for water-induced erosion is highest.

The during-S-1 flow path gradients (*Figure 12; B)* are also suggestive of a high erosive potential, however the presence of along-trail bicycle-induced ruts has limited the extent and connectedness of the vectors perpendicular to the trail axis when compared to the pre-S-1 flow

paths. The relatively large magnitude vectors terminated by point vectors on the right of the plot, indicate that flowing water may be impeded by the bicycle ruts and accumulate around and within. In addition to the slope on the right of the trail, the surface is also sloping down-trail (towards the top of the image). There are no significant gradients down-trail within the ruts suggesting a relatively uniform rut depth. The similar body weight and tire dimensions of the riders may contribute to this uniformity. Near the top of the study section there is an instance of flow path vector convergence which we believe to have been accommodated by a bicycle rut. More study is needed to better understand if along-slope rutting increases erosive potential through channelling.

The relaxation and smoothening of the surface after one week of reduced trail-use described in Sections 4.4 and 4.5 is evident when comparing the during-S-1 to the post-S-1 flow path gradients (*Figure 11; C*). The relative magnitude, alignment and gradient of the flow path vectors is reduced suggesting that post-S-1 a smoother and gentler sloping surface than pre-S-1 and during-S-1. Additionally, the overall radial distribution of flow path vectors perpendicular to the trail axis is less distinct than in the pre-S-1 and during-S-1 plots.

It was expected that most of the vectors in the during-S-1 plot would point downslope and focus within the ruts formed by cyclists however, no significant flow path vectors associated with the along-trail downslope (towards the top of the DEMs) were observed. We believe that the along trail grade was mistakenly redressed during orientation of the surface during the reconstruction stage, but maintained the slope perpendicular to trail axis because the model was aligned with the vertical concrete wall. Although our flow path models do not perfectly represent the trail surface, the ability to produce flow gradients from high resolution DEMs is important to future experimentation with this method.

4.7 Sinuosity

Mean sinuosity of trail transects (*Figure 13*), calculated from 3352 transects perpendicular to trail axis per surface, were used to compare roughness of the pre-S-1, during-S-1 and post-S-1 surfaces. This measurement follows from Jacques [2011], but in our case instead of a single transect, it is applied thousands of times down-axis of the trail. Incisions caused by bicycle tires, and foot and dog prints will tend to increase sinuosity whereas diffusion processes (material creep) between human disturbance events should serve to reduce sinuosity by smoothing the surface. A high mean sinuosity refers to a rougher surface, measured across a transect whereas a low mean sinuosity refers to a smoother surface[*Jacques*, 2011]. In general, increased sinuosity offers more opportunities for post-disturbance natural erosion by runoff. Large regions of roughness are shown by high-sinuosities that extends down-axis. The pre-S-1 surface exhibited the lowest mean sinuosity (1.09) while the post-S-1 surface, had the highest mean sinuosity (1.14). We expected the during-S-1 surface to have the highest sinuosity (1.13) given the abundance of ruts, however we believe that the saturated condition of the trail facilitated material creep, smoothing the surface and removing low-ampitude (<cm scale) roughness across much of the transects. The mean sinuosity of post-S-1 peaks sharply in three areas which we believe correspond to fresh dog paw prints easily recognisable in the reconstruction and DEM. These few rough features contributed significantly to the mean sinuosity. The differences in mean sinuosity between the surfaces is relatively small but likely significant given the small absolute values of sinuosity. We found that there was little change in

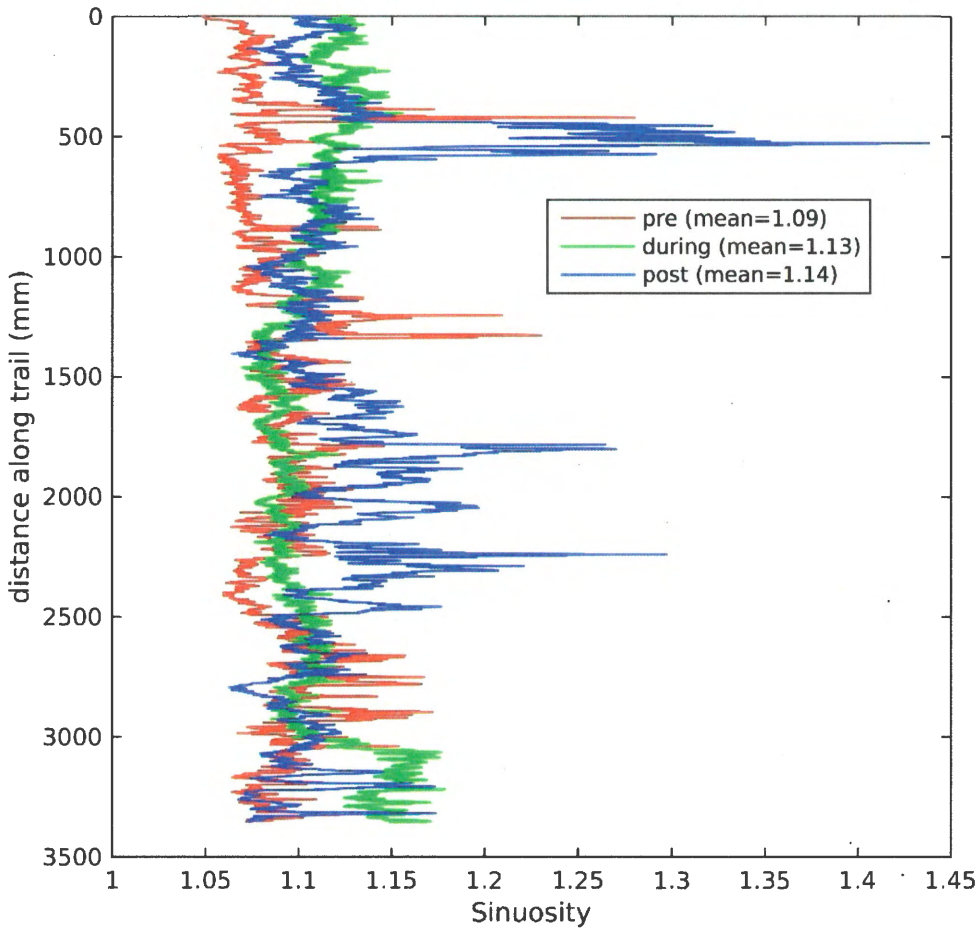

Figure 13. Sinuosities of the trail surface perpendicular to trail axis.

trail roughness between the unaltered and altered state, which compares to results found by Jacques [2011]. The increased frequency of cm-scale incisions by bicycle tires in the during-S-1 surface and dog paw prints in the post-S-1 surface increased the sinuosity of the surfaces albeit not significantly.

4.8 Height distribution function

The height distribution functions of the pre-S-1, during-S-1 and post-S-1 surfaces were calculated and plotted for comparison (*Figure 14*). In other fields of study, surface microirregularities are measured on extremely smooth surfaces such as experimental-grade

optical lenses and plotted as height distribution functions. Their "signatures" (probability peaks occurring for similar elevations) classify the effectiveness of roughness causing specular and non-specular scattering. We found that the height distribution functions of pre-S-1, during-S-1 and post-S-1 have similar signatures and their root-mean squares are comparable (26.5082, 26.9200 and 26.9246 respectively). The similarity of the height distribution functions suggests

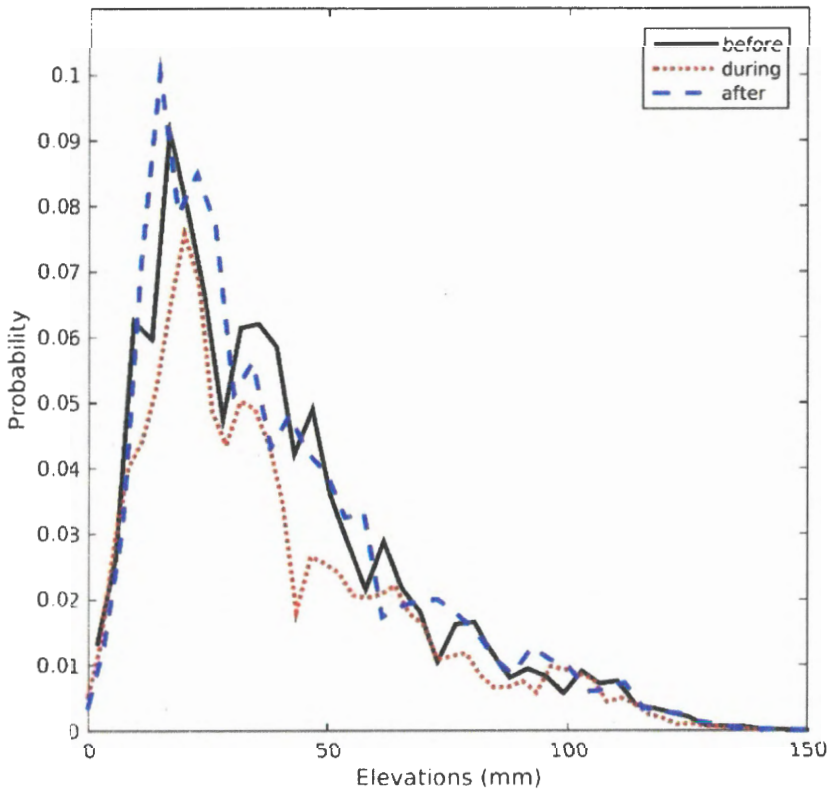

Figure 14. Height distribution functions of pre-S-1, during-S-1 and post-S-1.

that the surface did not change very much over the test period. The overall probability of large elevations is greatest for post-S-1, less so for pre-S-1, and even less than for during-S-1. We believe that the variability in elevation probability of the surfaces is not significant enough in order to correlate surface expressions of trail impacts with height distribution function signature shape with certainty.

4.9 Recommendations for future work

Our analysis method, using structure-from-motion photogrammetry and statistical software, and results thereof can be improved by modifying some key components in the process. Initial experimentation with various software was limited by computing power and therefore obtaining results quickly was difficult. We recommend using the most powerful hardware available. Comparison of flow path gradients calculated in Section 4.6 with qualitative observations made of the surface suggest that along-trail downslope data was mistakenly redressed, probably during the manual model reorientation process prior to reconstruction. We recommend using at least five easily identifiable GCPs outside the bounds of the study area and recording their spatial locations using differential GPS. When measuring a sloping surface, it is important to accurately measure the elevation of the GCPs as well as their location. This avoids estimating the surface orientation using a local coordinate system in Agisoft Photoscan Professional and ensures that a consistent reference datum is used. Nonetheless, the ability to produce sub-millimeter accuracy DEMs of trail surfaces using SfM will be an important advancement for future developments in trail analysis.

5.0 Conclusion

Our mm-scale DEMs and DODs from York Redoubt, and the several analysis methods we applied to these, support our hypothesis that structure-from-motion photogrammetry can be used to record changes of trails at the mm-scale. DODs showed that material within the system is locally redistributed rather than significantly removed or added although a small net-soil loss was measured. It is possible that over large areas this effect may be cumulative and with additional influences from climate, substrate variability and vegetation may result in more

significant soil loss. Trail roughness changes in response to user disturbances (mostly cyclists in this case) showed that impacts were variable on both across- and down-trail axes (shown by transect mean elevation changes and first standard deviation). Bulk measurements of the entire trail surface, such as total mean sinuosity and the HDF (height distribution function) showed very little change over time, despite the significant local changes revealed by local sinuosity. Based on this, we suggest that region-specific metrics will be important tools to quantifying change and making trail management decisions, whereas measurements that integrate across a large trail surface will not. Our methods and results were not intended to test the effects of different types or numbers of users, but SfM shows promise as a method of examining such effects.

References

Brubaker, K. M., W. L. Myers, P. J. Drohan, D. A. Miller, and E. W. Boyer (2013), The use of LiDAR terrain data in characterizing surface roughness and microtopography, *Appl. Environ. Soil Sci.*, *2013*, doi:10.1155/2013/891534.

Cole, D. N., and C. A. Monz (2004), Spatial patterns of recreation impact on experimental campsites, *J. Environ. Manage.*, *70*(1), 73–84, doi:10.1016/j.jenvman.2003.10.006.

Columbia University (1999), SfM Origins: Photogrammetry and Early Vision, Available from: http://www.cs.columbia.edu/~jebara/htmlpapers/SFM/node4.html (Accessed 27 October 2015)

Dietrich, J. T. (2015), Riverscape mapping with helicopter-based Structure-from-Motion photogrammetry, *Geomorphology*, *252*, 144–157, doi:10.1016/j.geomorph.2015.05.008.

Growcock, A. J. W. (2005), Impacts of Camping and Trampling on Australian Alpine and Subalpine Vegetation and Soils, , (October).

Jacques, I. J. (2011), Trail Degradation on the Nine Mile Trail System, Nova Soctia: The Effects of Users on Trail Compaction and Rutting, Dalhousie University.

Lambin, E. F. et al. (2001), The causes of land-use and land-cover change: Moving beyond the myths, *Glob. Environ. Chang.*, *11*(4), 261–269, doi:10.1016/S0959-3780(01)00007-3.

Leon, J. X., C. M. Roelfsema, M. I. Saunders, and S. R. Phinn (2014), Measuring coral reef terrain roughness using "Structure-from-Motion" close-range photogrammetry, *Geomorphology*, *242*, 21–28, doi:10.1016/j.geomorph.2015.01.030.

Létourneau, G. (2010), Land Cover Along the Great Lakes and the St. Lawrence River, Available from: http://planstlaurent.qc.ca/fileadmin/site_documents/documents/PDFs_accessibles/Occupation_e_FINAL_v1.0.pdf (Accessed 12 February 2016)

Leung, Y. F., and J. L. Marion (1999), The influence of sampling interval on the accuracy of trail impact assessment, *Landsc. Urban Plan.*, *43*(4), 167–179, doi:10.1016/S0169-2046(98)00110-8.

Lewis, A., G. E. Hilley, and J. L. Lewicki (2015), Integrated thermal infrared imaging and structure-from-motion photogrammetry to map apparent temperature and radiant hydrothermal heat flux at Mammoth Mountain , CA , USA, *J. Volcanol. Geotherm. Res.*, *303*, 16–24, doi:10.1016/j.jvolgeores.2015.07.025.

Maller, C., M. Townsend, L. S. Leger, C. Henderson-wilson, A. Pryor, L. Prosser, and M. Moore (2010), Healthy Parks , Healthy People : The Health Benefits of Contact with Nature in a Park Context, *George Wright Forum*, *26*(2), 51–83.

Marion, J. L. (2006), Assessing and Understanding Trail Degradation : Results from Big South Fork National River and Recreational Area, *Wildl. Res.*, 84.

Maybank, S. (1993), *Theory of Reconstruction from Image Motion*, 1st ed., Springer Berlin Heidelberg, Berlin.

Olive, N. D., and J. L. Marion (2009), The influence of use-related, environmental, and managerial factors on soil loss from recreational trails, *J. Environ. Manage.*, *90*(3), 1483–1493, doi:10.1016/j.jenvman.2008.10.004.

Pickering, C. M., S. Rossi, and A. Barros (2011), Assessing the impacts of mountain biking and

hiking on subalpine grassland in australia using an experimental protocol, *J. Environ. Manage.*, *92*(12), 3049–3057, doi:10.1016/j.jenvman.2011.07.016.

Slama, C. C. (Ed.) (1980), *Manual of Photogrammetry*, 4th ed., American Society of Photogrammetry and Remote Sensing, Falls Church.

Tomczyk, A. M., and M. Ewertowski (2012), Quantifying short-term surface changes on recreational trails: The use of topographic surveys and "digital elevation models of differences" (DODs), *Geomorphology*, *183*, 58–72, doi:10.1016/j.geomorph.2012.08.005.

Westoby, M. J., J. Brasington, N. F. Glasser, M. J. Hambrey, and J. M. Reynolds (2012), "Structure-from-Motion" photogrammetry: A low-cost, effective tool for geoscience applications, *Geomorphology*, *179*, 300–314, doi:10.1016/j.geomorph.2012.08.021.

White, D. D., M. T. Waskey, G. P. Brodehl, and P. E. Foti (2006), A Comparative Study of Impacts to Mountain Bike Trails in Five Common Ecological Regions of the Southwestern U . S ., *J. Park Recreat. Admi.*, *24*(2), 21–42.

Wilson, J. P., and J. P. Seney (1994), Erosional of Hikers , Impact and Off-Road Bicycles Trails, *Society*, *14*(1), 77–88.